Highlights

Sulfate limitation increases specific plasmid DNA yield in *E. coli* fed-batch processes

Mathias Gotsmy,Florian Strobl,Florian Weiß,Petra Gruber,Barbara Kraus,Juergen Mairhofer,Jürgen Zanghellini

- Genome-scale metabolic models predict growth decoupling strategies
- Sulfate limitation decouples cell growth from pDNA production
- Sulfate limitation increases the specific supercoiled pDNA yield by 29 % without loss of quality

Sulfate limitation increases specific plasmid DNA yield in *E. coli* fed-batch processes

Mathias Gotsmy[a,b], Florian Strobl[c], Florian Weiß[c], Petra Gruber[d], Barbara Kraus[d], Juergen Mairhofer[c] and Jürgen Zanghellini[a,*]

[a]*Department of Analytical Chemistry, University of Vienna, Vienna, 1090, Austria*
[b]*Doctorate School of Chemistry, University of Vienna, Vienna, 1090, Austria*
[c]*enGenes Biotech GmbH, Vienna, 1190, Austria*
[d]*Baxalta Innovations GmbH, A Part of Takeda Companies, Orth an der Donau, 2304, Austria*

ARTICLE INFO

Keywords:
growth decoupling
medium optimization
GSMM
FBA
dFBA
E. coli
plasmid production

ABSTRACT

Plasmid DNA (pDNA) is a key biotechnological product whose importance became apparent in the last years due to its role as a raw material in the messenger ribonucleic acid (mRNA) vaccine manufacturing process. In pharmaceutical production processes, cells need to grow in the defined medium in order to guarantee the highest standards of quality and repeatability. However, often these requirements result in low product titer, productivity, and yield.

In this study, we used constraint-based metabolic modeling to optimize the average volumetric productivity of pDNA production in a fed-batch process. We identified a set of 13 nutrients in the growth medium that are essential for cell growth but not for pDNA replication. When these nutrients are depleted in the medium, cell growth is stalled and pDNA production is increased, raising the specific and volumetric yield and productivity. To exploit this effect we designed a three-stage process (1. batch, 2. fed-batch with cell growth, 3. fed-batch without cell growth). The transition between stage 2 and 3 is induced by sulfate starvation. Its onset can be easily controlled via the initial concentration of sulfate in the medium.

We validated the decoupling behavior of sulfate and assessed pDNA quality attributes (supercoiled pDNA content) in *E. coli* with lab-scale bioreactor cultivations. The results showed an increase in supercoiled pDNA to biomass yield by 29 % upon limitation of sulfate.

In conclusion, even for routinely manufactured biotechnological products such as pDNA, simple changes in the growth medium can significantly improve the yield and quality.

1. Introduction

Plasmid DNA (pDNA) is an important product of the pharmaceutical industry being primarily used as vectors for the transfection of mammalian cells. For example, pDNA can be directly injected in the form of a DNA vaccine [1]. Moreover, it is an important raw material for the production of mRNA vaccines, for example against SARS-CoV-2 [2, 3]. Additionally, pDNA can be used as a vector for gene therapy [4]. Regardless of the application, high amounts and high quality of pDNA are needed and the optimization of its production is of health-economic interest as pDNA is a relevant driver of manufacturing costs.

Apart from solely maximizing the yield of pDNA, three prerequisites are required for the design of a pDNA production process. Firstly, pDNA can be present in an open circular (oc), linear (l), or covalently closed circular (ccc) supercoiled form. However, the ccc form is generally considered more favorable for transfection of mammalian cells and, therefore, the fraction of supercoiling is of importance [5, 6]. Secondly, a loss of plasmid can be severely detrimental to the productivity during the fermentation process. Classically, this problem can be mitigated by the introduction of antibiotic resistance selection systems and the usage of antibiotic selection pressure during fermentation. However, these systems have several downsides. They, on the one hand, shift metabolic resources from the production of pDNA to the production of antibiotic resistance proteins [7]. On the other hand, special care has to be taken to remove residual antibiotics during pDNA purification and the absence thereof has to be validated. Therefore, several alternatives have been developed [8] although still not state-of-the-art yet for pDNA manufacturing. Thirdly, even though pDNA production in complex media generates higher yields, chemically defined media are preferred for the production of high-quality and safe pharmaceuticals [1].

Many strategies for the increase of pDNA production have been published with a large fraction using *E. coli* as production organism [9]. The methods range from the screening of favorable strains to metabolic engineering through knocking-in and -out of genes to antibiotic-free selection systems and other highly optimized production strains [9]. Most strategies for increasing pDNA production can be grouped into two conceptual approaches: (i) the reduction of cell growth; (ii) ensuring a constant supply of DNA precursor metabolites. The methods differ widely in the way one (or both) aims are achieved.

Early on researchers found that a low growth rate increases the specific productivity of pDNA [10]. To achieve this in batch fermentations Galindo et al. [11] designed a

*Corresponding author
ORCID(s): 0000-0003-1333-4870 (M. Gotsmy); 0000-0002-2686-1971 (J. Mairhofer); 0000-0002-1964-2455 (J. Zanghellini)

medium that releases glucose enzymatically and thus downregulates glucose uptake and subsequently growth. Alternatively, Soto et al. [12] developed *E. coli* strain VH33 by knocking-out the main uptake pathway of glucose to achieve the same result. With this method, they could increase the production to 40 mg L^{-1} pDNA compared to 17 mg L^{-1} of the wild type strain [12]. Moreover, an optimization strategy for microaerobic environments was devised where *E. coli* strain W3110 improved pDNA production in presence of a recombinant expression of the *Vitreoscilla* hemoglobin protein [13]. In a subsequent study, this strain was tested in batch fermentations with different oxygen transfer rates and they concluded that as oxygen was depleted the growth rate decreased and the production of pDNA increased [14].

A strategy to ensure a constant supply of DNA precursor metabolites is, for example, the knocking-out of pyruvate kinase which forces metabolization of glucose over the pentose phosphate pathway [7, 15, 16]. Other methods utilize stoichiometric models to optimize the growth medium [17]. These authors concluded that the addition of the nucleosides adenosine, guanosine, cytidine, and thymidine as well as several amino acids can significantly improve pDNA production (60 mg L^{-1} in a batch fermentation). Martins et al. [18] optimized the growth medium for the high producer strain VH33 and concluded that the presence of aromatic amino acids (phenylalanine, tryptophan, tyrosine) is advantageous for redirecting molecules to the nucleotide synthesis pathways. Additionally, the effect of the amount and type of nitrogen source in the growth medium has been investigated on the production of pDNA to 213 mg L^{-1} [19]. Also, economical aspects of the medium design have been discussed [20].

Further potential for optimization is the pDNA itself. For example, reducing the size of the pDNA has been linked to higher volumetric yields [21]. However, a reduction might not always be possible, especially for therapeutic applications, where plasmid sizes are typically large (> 6 kb) [22]. Moreover, the pDNA yield of a process is highly dependent on the origin of replication (ORI). Currently, most plasmids carry a high copy number pUC ORI that allows up to 700 pDNA copies per cell [1]. Other approaches involved heat-induced origins of replication that increase the plasmid copy number at higher temperatures than 37 °C [23, 24]. However, higher temperatures come with physiological trade-offs and therefore the amplitude and timing of heat induction are of importance [25].

Recently also other production organisms were proposed, e.g. *Lactococcus lactis*. In contrary to *E. coli*, *L. lactis* is generally regarded as safe (GRAS) and thus simplifies the downstream processing [26, 27].

Here, we design a three-stage bioprocess, where cellular growth and pDNA production are decoupled. We use constraint-based modeling to (i) identify medium components that induce the switching and (ii) determine the optimal time point for switching between the phases such that the average volumetric productivity is maximized.

2. Methods

2.1. Metabolic Modeling

2.1.1. Model Creation

For our analysis, we used *i*ML1515 [28], a genome-scale metabolic model of *Escherichia coli* strain K-12 substrain MG1655. All model modifications and simulations were performed in Python 3.10 using the CobraPy package [29].

To simulate plasmid production, a 8 base pair dummy pDNA metabolite with 50 % GC content was added to the model. Subsequently, we added a pDNA production reaction, corresponding to the dummy plasmid's stoichiometry. pDNA polymerization cost was estimated to 1.36 mol adenosine triphosphate (ATP) per mol dNTP [7, 30]. Additionally, a pDNA sink reaction was introduced to make fluxes through the pDNA synthesis reaction feasible. An SBML version of the used model is available at `https://github.com/Gotsmy/slim/tree/main/models`.

Although 8 bp is an unrealistically small size for a real pDNA molecule, we emphasize that the actual length of the plasmid does not change the relative underlying stoichiometry. Moreover, the dummy plasmid already has a molecular weight of approximately 4943.15 g mol^{-1}. Including a longer pDNA molecule cannot realistically change the results, however, as molecular weights become larger, the flux values become very small, which could lead to numerical instabilities during simulation.

2.1.2. Identification of Decoupling Compounds

Initially, we performed a parsimonious flux balance analysis (pFBA) [31] with biomass growth as objective. The maximal glucose uptake rate was set to 10 mmol g^{-1} h^{-1} and a non-growth associated maintenance requirement was set to 6.86 mmol ATP g^{-1} h^{-1} [28]. Exchange reactions with non-zero fluxes were used for the definition of the minimal medium. All exchange reactions that were not present in the minimal medium, except for H_2O and H^+, were turned off. To investigate the differences in uptake fluxes, an additional pFBA was performed with pDNA as the objective.

Next, we selected each of the minimal medium components and set the maximum exchange flux bound for this metabolite to 5, 25, 50, 75, and 100 % of the flux during biomass growth. For each value, a production envelope (pDNA synthesis as a function of growth) was calculated. Decoupling medium components were identified as metabolites which, as their uptake flux decreased, the maximum pDNA synthesis potential increased at a maximum biomass growth.

2.1.3. Dynamic Flux Balance Analysis

We used dynamic flux balance analysis (dFBA) [32] to simulate batch and fed-batch processes. At every integration step, a lexicographic flux balance analysis (FBA), where all fluxes of interest were consecutively optimized, was performed [33]. The list of objectives is given in Table 1. We used SciPy's `solve_ivp` function for numerical integration [34].

Table 1
Lexicographic objectives for dFBA. The order of optimization was top to bottom.

	Objective
max	biomass production
min	sulfate uptake
max	pDNA production

Sulfate concentration in the medium was tracked as its depletion coincides with the metabolic switch from biomass growth to production. Due to a lack of knowledge, no uptake kinetics of sulfate were simulated. Instead, the exchange reaction bounds were left unconstrained when $C_{SO_4^{2-}}(t) > 0$ and were blocked when $C_{SO_4^{2-}}(t) \leq 0$.

High copy number origin of replication plasmids typically replicate during the growth phase as they high-jack genomic DNA synthesis pathways. Therefore, we set a lower bound, $q^{\mu}_{\text{pDNA}} = 4.9\,\text{mg}\,\text{g}^{-1}\,\text{h}^{-1}$, for the pDNA synthesis reaction. Moreover, it is unrealistic to assume that all available glucose is channeled towards pDNA production during the SO_4^{2-} starvation. Therefore, we set an upper bound to the synthesis reaction. Since its actual value was unknown, we tested several levels ranging from $q^{*}_{\text{pDNA}} = 4.9$ to $24.7\,\text{mg}\,\text{g}^{-1}\,\text{h}^{-1}$. Throughout this manuscript, that ratio of upper to lower bound of the pDNA synthesis reaction is referred to as

$$\kappa_{\text{pDNA}} = {q^{*}_{\text{pDNA}}}/{q^{\mu}_{\text{pDNA}}}. \tag{1}$$

We performed simulations in 41 equidistant levels of $\kappa_{\text{pDNA}} \in [1, 5]$. Because of the implementation of the dFBA, the lower and upper bounds of the synthesis reaction can be interpreted as the pDNA synthesis fluxes during the growth and SO_4^{2-} starvation phase, respectively. We assumed negligible changes in overall biomass composition due to pDNA synthesis, which solely derives from external carbon sources.

To compare pDNA production processes, we calculated two performance indicators: the specific yield

$$Y_{\text{pDNA/biomass}}(t) := {C_{\text{pDNA}}(t)}/{C_{\text{biomass}}(t)}, \tag{2}$$

and the average volumetric productivity

$$p_{\text{pDNA}}(t) := \frac{C_{\text{pDNA}}(t) - C_{\text{pDNA}}(t_0)}{t - t_0}. \tag{3}$$

Batch Process Initial conditions (Table 2) represent a realistic batch process in a small bioreactor. Glucose uptake rate, $q_{\text{glucose}}(t)$, was modeled as Michaelis-Menten kinetics,

$$q_{\text{glucose}}(t) = \frac{q^{\max}_{\text{glucose}} C_{\text{glucose}}(t)}{k_{\text{M}} + C_{\text{glucose}}(t)} \tag{4}$$

with C_{glucose} denoting the current glucose concentration in the medium, and two constants ($q^{\max}_{\text{glucose}}, k_{\text{M}}$). Simulations terminated once the glucose concentration dropped below the level of what was required for ATP maintenance. Initial sulfate concentration was varied in 301 equidistant steps to search for a volumetric pDNA productivity optimum.

Table 2
Parameters for dFBA simulations. Cells marked with "–" are not applicable and cells marked with "var" are not constant in the respective process.

		fed-batch		
parameter	batch	exponential	linear	unit
$C_{\text{biomass}}(0)$	0.02	3.04	3.04	$\text{g}\,\text{L}^{-1}$
$C_{\text{glucose}}(0)$	20	0	0	$\text{g}\,\text{L}^{-1}$
$C_{SO_4^{2-}}(0)$	0 ... 0.29	0 ... 3.8	0 ... 2.9	$\text{g}\,\text{L}^{-1}$
$C_{\text{pDNA}}(0)$	0	0	0	$\text{g}\,\text{L}^{-1}$
$C^{\text{feed}}_{\text{glucose}}$	–	330	330	$\text{g}\,\text{L}^{-1}$
$V(0)$	0.5	0.5	0.5	L
$V(t_{\text{end}})$	0.5	1	1	L
t_{end}	var	35.2	36.0	h
k_{M}	2.7 [35]	–	–	$\text{mg}\,\text{L}^{-1}$
μ	var	0.1	var	h^{-1}
$q^{\max}_{\text{glucose}}$	1.9 [36]	–	–	$\text{g}\,\text{g}^{-1}\,\text{h}^{-1}$
q^{μ}_{pDNA}	4.9	4.9	4.9	$\text{mg}\,\text{g}^{-1}\,\text{L}^{-1}$
q_{ATPM}	6.86	6.86	6.86	$\text{mmol}\,\text{g}^{-1}\,\text{h}^{-1}$
r^{feed}_{i}	–	13.9	Eq. (5)	$\text{mL}\,\text{h}^{-1}$
$Y_{\text{feed/biomass}}$	–	10	–	$\text{mL}\,\text{g}^{-1}$

Fed-Batch Process Initial conditions resembled realistic values from the end of a batch process in a small bioreactor (Table 2). Strategies with a linear (i.e. constant) feeding rate, $r^{\text{feed}}_{\text{lin}}$, and an exponential feeding rate,

$$r^{\text{feed}}_{\text{exp}} = \mu C_{\text{biomass}}(0) V(0) Y_{\text{feed/biomass}} \exp(\mu t), \tag{5}$$

were tested. The specific glucose uptake rate was set to

$$q_{\text{glucose}}(t) = \frac{r^{\text{feed}} C^{\text{feed}}_{\text{glucose}}}{C_{\text{biomass}}(t) V(t)} \tag{6}$$

to ensure $C_{\text{glucose}} = 0$ throughout the (non-starved) fed-batch phase. Here, $C^{\text{feed}}_{\text{glucose}}$ denotes the glucose concentration in the feed medium.

The dFBA simulation terminated once the maximal volume of 1 L was reached (i.e. after 35.2 and 36.0 h in exponential and linear fed-batch, respectively). Similar to the batch process, the initial sulfate concentration in the medium was varied in 301 equidistant steps to search for a productivity optimum. We assumed that sulfate was present in the medium at the start of the feed, while the feed medium was sulfate free.

All code used for the creation, simulation, and analysis of the model is available at `https://github.com/Gotsmy/slim`.

2.2. Validation Experiments

2.2.1. Upstream Process

All experiments were conducted with proline auxotroph *E. coli* K-12 strain JM108 [37], which previously had been

used for pDNA production [8]. The cells were transformed with a plasmid of 12.0 kbp length, 53 % GC content containing a kanamycin resistance gene.

For fed-batch fermentations, *E. coli* JM108 were grown in a 1.8 L (1.0 L net volume, 0.5 L batch volume) computer-controlled bioreactor (DASGIP parallel bioreactor system, Eppendorf AG, Germany). The bioreactor was equipped with a pH probe (Hamilton Bonaduz AG, Switzerland) and an optical dissolved oxygen probe (Hamilton Bonaduz AG). The pH was maintained at 7.0 ± 0.1 by addition of 12.5 % ammonia solution; the temperature was maintained at 37.0 ± 0.5 °C. The dissolved oxygen (O_2) level was stabilized above 30 % saturation by controlling the stirrer speed, aeration rate, and gassing composition. Foaming was suppressed by the addition of 2 mL 1:10 diluted Struktol J673A antifoam suspension (Schill+Seilacher, Germany) to the batch medium and by the automatic addition of 1:10 diluted Struktol J673A controlled by a conductivity-operated level sensor. For the inoculation of the bioreactor, a seed culture was used (25 mL batch medium inoculated with 250 µL master cell bank in 250 mL baffled glass flasks at 37 °C with shaking at 180 rpm). Seed culture was incubated until a final OD_{600} of 2-4 was reached and a defined volume was transferred aseptically to the bioreactor to result in an initial OD_{600} of 0.015.

The fermentation process was designed for a final amount of 50 g cell dry mass (CDM) of which 1.51 g was obtained in a batch volume of 500 mL and 48.5 g during the feed phase via the addition of another 500 mL of feed medium. The amount of glucose for the specific medium was calculated based on a yield coefficient ($Y_{\text{biomass/glucose}}$) of 0.303 g g^{-1} and added as $C_6H_{12}O_6 \cdot H_2O$. For media preparation, all chemicals were purchased from Carl Roth GmbH (Germany) unless otherwise stated. Two different media compositions were compared regarding specific pDNA productivity: one with a limited sulfur source (SO_4^{2-}-limitation) and one without a limited sulfur source (control). Feeding was initiated when the culture in the batch medium entered the stationary phase. A fed-batch regime with a linear substrate feed (0.26 g min^{-1} respectively 13.91 mL h^{-1}) was used for 35 h (approximately five generations). During SO_4^{2-}-limitation fermentations, the provided sulfur was completely consumed at 23 h after feed start. The batch and fed-batch medium components are given in Supplementary Table S1. The cultivations of SO_4^{2-}-limitation and control were conducted in triplicates.

2.2.2. Analysis

For off-line analysis (OD_{600}, CDM, pDNA product), the bioreactor was sampled during the fed-batch phase. The OD_{600} was measured using an Ultrospec 500 pro Spectrophotometer (Amersham Biosciences, UK), diluting the samples with phosphate-buffered saline to achieve the linear range of measurement. For the determination of CDM, 1 mL of cell suspension was transferred to pre-weighed 2.0 mL reaction tubes and centrifuged for 10 min at 16.100 rcf and 4 °C with an Eppendorf 5415 R centrifuge. The supernatant was transferred to another reaction tube and stored at −20 °C for further analysis. As a washing step, the cell pellet was resuspended in 1.8 mL RO-H_2O, centrifuged, and the supernatant discarded. Afterwards, the pellet was resuspended in 1.8 mL RO-H_2O and finally dried at 105 °C for 24 h. The reaction tubes with the dried biomass were cooled to room temperature in a desiccator before re-weighing.

For pDNA product analysis, the sampling volume of the cell suspension, corresponding to 20 mg CDM, was estimated via direct measurement of the OD_{600}. The calculated amount was transferred to 2.0 mL reaction tubes and centrifuged at 16.100 rcf and 4 °C for 10 min. The supernatant was discarded, and the cell pellets were stored at −20 °C.

The content of pDNA in ccc-conformation was determined using AIEX-HPLC (CIMac™ pDNA-0.3 Analytical Column, 1.4 µL; BIA Separations d.o.o., Slovenia). For HPLC analysis cell disintegration was performed by an alkaline lysis method [38]. The obtained lysate was directly analyzed by HPLC (Agilent 1100 with a quaternary pump and diode-array detector (DAD)). Values derived from three biological replicates have a coefficient of variation lower than 10 %.

The average volumetric productivity ($p_{\text{pDNA}}(t)$) and the average specific yield ($Y_{\text{pDNA/biomass}}(t)$) were calculated as given in Equations (3) and (2), respectively. The time-dependent pDNA synthesis rate ($q_{\text{pDNA}}(t)$) was estimated via the `finitediff` Python package [39, 40].

3. Results

3.1. Key Objective

We aim to design an efficient two-phase fermentation process for pDNA production in *E. coli*, where cellular growth and pDNA production are separated.

In the following, we will

(i) use constraint-based modeling to identify medium components that enable switching from growth to production phase;

(ii) determine optimal switching time points to maximize the average productivity in a batch and fed-batch fermentation; and

(iii) experimentally validate the computed strategies in a linear fed-batch process.

3.2. Identification of Decoupling Compounds

First, we used pFBA to compute a minimal set of uptake rates in the genome-scale metabolic model *i*ML1515 [28] supporting maximal aerobic growth of *E. coli* with glucose as carbon source. Similarly, we computed uptake rates for maximal pDNA production using the same constraints (Figure 1). All calculated uptake rates are inflexible in the optima, except for Fe^{2+} and O_2. Their uptake can be further increased by conversion to and excretion of Fe^{3+} and H_2O. In contrast to biomass synthesis, pDNA production requires only glucose, O_2, NH_4^+, and HPO_4^{2-}, but no further nutrients. Therefore, we conclude that these remaining nutrients could

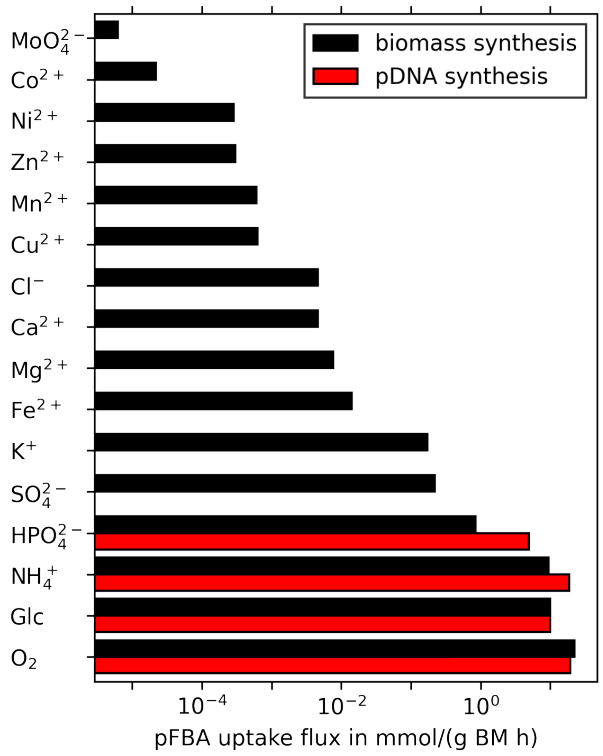

Figure 1: pFBA uptake flux rates for all minimal medium components. Black bars represent fluxes for optimization of biomass synthesis, red bars represent fluxes of pDNA synthesis.

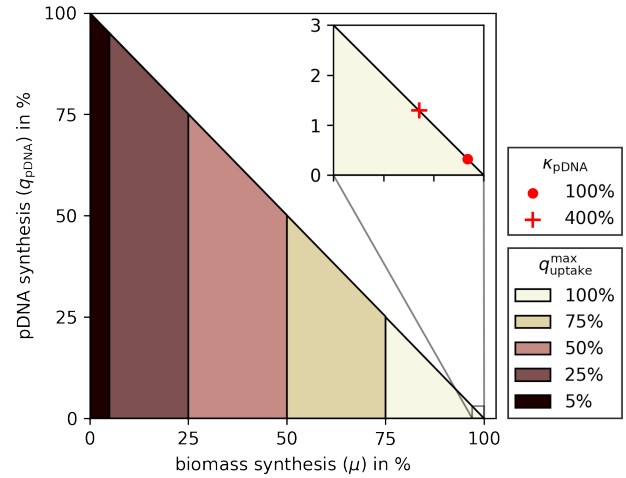

Figure 2: Normalized pDNA production envelopes for different maximal uptake rates of (a single) decoupling nutrient. Ca^{2+}, Cl^-, Co^{2+}, Cu^{2+}, Fe^{2+}, K^+, Mg^{2+}, Mn^{2+}, MoO_4^{2-}, Ni^{2+}, SO_4^{2-}, and Zn^{2+} all result in identical sets of production envelopes. Note that all production envelopes include the line segment from (0|0) to (0|100). The inset shows the extreme points of a production envelope with a realistic pDNA production rate during biomass growth (red circle) and a potential 4-fold pDNA production rate increase (red cross).

potentially be used as decoupling agents separating pDNA synthesis from growth.

Next, for each decoupling nutrient, we restricted its uptake between zero and 100 % of its rate at maximum growth and computed the corresponding pDNA production envelopes as a function of growth (Figure 2). All twelve decoupling nutrients result in identical sets of production envelopes, which mirrors the fact that each decoupling nutrient is essential for growth but not required for pDNA production. Note that the one-to-one trade-off between biomass production and pDNA synthesis, i.e., the upper limit of the production envelope, is a straight line between the points (0|100) and (100|0).

Realistically, pDNA production rates are significantly less than the theoretical value of 100 % in Figure 2. Therefore, in the inset of the same figure, the red markers illustrate the extreme points of more reasonable production envelopes. For example, the red circle (i.e., $\kappa_{pDNA} = 100\,\%$) illustrates average rates of pDNA production during cell growth. Even when the decoupling would lead to a boost by a factor of $\kappa_{pDNA} = 4$ (red cross), the resulting pDNA production flux would be only 1.3 % of the theoretical maximum.

In the following, we focus on the impact of the six bulk non-metal elements (sulfur, phosphorus, oxygen, nitrogen, carbon, and hydrogen) that typically make up 97 % (g g^{-1}) of the elemental biomass composition [41]. Moreover, except for potassium (and sulfate), all other predicted decoupling nutrients (iron, magnesium, calcium, chlorine, copper, manganese, zinc, nickel, cobalt, and molybdenum) are taken up at minute rates ($< 15\,\mu mol\,g^{-1}\,h^{-1}$, Figure 1). Thus, exactly dosing their concentrations for limitation may be challenging in a bio-process. This leaves sulfate as the only predicted decoupling nutrient in a glucose-minimal medium.

3.3. Optimal Sulfate-Limited Processes

Decoupling production from growth during a bio-process raises the question of timing: when to best switch from growth to production phase to maximize performance.

In the following, we used dFBA [32] to track the time-dependent concentrations $C_i(t)$ of biomass, pDNA, glucose, and sulfate and determine the optimal initial sulfate concentration, $C_{SO_4^{2-}}(0)$, that maximize the average volumetric productivity

$$\max_{C_{SO_4^{2-}}(0)} p_{pDNA}\left(t_{end}, C_{SO_4^{2-}}(0)\right) \tag{7}$$

in a batch and fed-batch process. Here t_{end} denotes the end of the bio-process, which terminates when either glucose is consumed (batch) or the maximal volumetric capacity of the reactor is reached (fed-batch). Our simulations assume that pDNA production occurs (i) at a constant rate $q^*_{pDNA} = \kappa_{pDNA} q^{\mu}_{pDNA}$ during the sulfate starvation phase; (ii) at q^{μ}_{pDNA} during the growth phase.

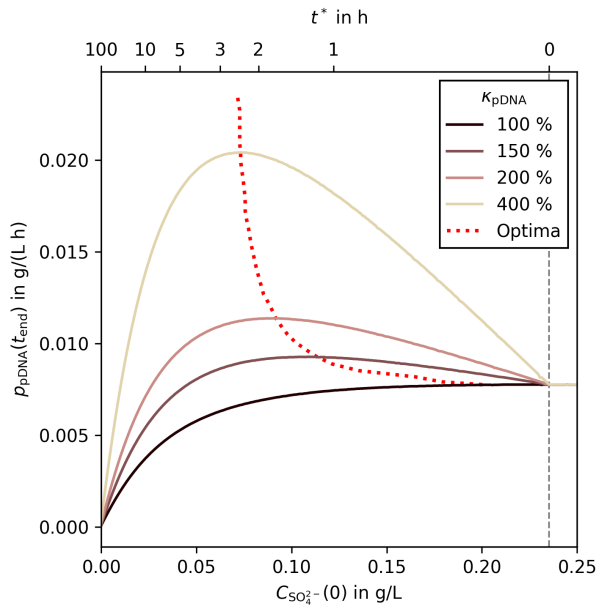

Figure 3: Predicted optimal timing in a SO_4^{2-}-limited batch process. The panel shows average volumetric productivities of pDNA production ($g\,L^{-1}\,h^{-1}$) as a function of the initial SO_4^{2-} concentration in a batch process. The full lines represent different levels of increased pDNA production during starvation as percentages of pDNA production rate during biomass growth (κ_{pDNA}). The dotted line indicates the moving average of the location of the optima for κ_{pDNA} between 100 and 500 %. The second X-axis of the figure (top) illustrates the length of the sulfate-starved process phase (t^*). For all modeled batch processes, right of the gray dashed line, no SO_4^{2-} limitation occurred. The process curves of an optimal batch are shown in Supplementary Figure S1.

3.3.1. *Batch Process*

We simulated sulfate-limited batch processes using the initial values listed in Table 2 and analyzed the impact of the length of the pDNA production phase (induced by sulfate starvation) on the average volumetric productivity (Figure 3).

We observe distinct maxima in the average volumetric productivity when $\kappa_{pDNA} > 1$ (red dotted line, Figure 3), i.e. when the pDNA production rate is enhanced. With increasing κ_{pDNA}, the maximum productivity increases and moves towards smaller values of $C_{SO_4^{2-}}(0)$. The initial sulfate concentration in Figure 3 is an indicator of the length of the growth phase. The larger $C_{SO_4^{2-}}(0)$, the longer the growth phase and the shorter the pDNA production phase, and vice versa (second X-axis, top of Figure 3). Thus, Figure 3 mirrors the trade-off between producing a sufficiently high cell density that catalyzes the synthesis of pDNA, and actual pDNA production [42]. For large improvements, i.e., $\kappa_{pDNA} \gtrapprox 3$, the optimal length of the starvation phase is roughly 2.5 h and becomes virtually independent of κ_{pDNA}.

As an example, the optimal productivity for $\kappa_{pDNA} = 2$ (corresponding to $q^*_{pDNA} = 9.9\,mg\,g^{-1}\,h^{-1}$) is reached by adding $0.092\,g\,L^{-1}$ SO_4^{2-} into the batch medium. This results in a 1.7 h starvation phase, which increases the average volumetric productivity by 47 %. The time-dependent concentrations of this process are shown in Figure S1A and B.

3.3.2. *Fed-batch Process*

Next, we simulated sulfate-limited fed-batch processes with a linear feed using the values listed in Table 2. In all simulations the feed rate was constant. Thus, in contrast to the batch process analyzed above, here, the process length is always 36 h. Subsequently, we analyzed the impact of the length of the pDNA production phase (induced by sulfate starvation during the feed phase) on the average volumetric productivity.

Similar to the batch process, we again observe distinct maxima in the average volumetric productivity when $\kappa_{pDNA} > 1$ (red dotted line, Figure 4A). However, now the maxima occur at much longer starvation times compared to the batch process ($t^* = 19$ h versus 2.5 h at $\kappa_{pDNA} = 4$). Even compared to an equivalent exponential fed-batch (see Section 2.1.3 for design details of this process), the optimal starvation is longer in a linear than in an exponential fed-batch process (Supplementary Figure S3) For instance, at $\kappa_{pDNA} = 1.5$ a linear fed-batch process achieves an optimal $p_{pDNA} = 0.18\,g\,L\,h$ at $t^* = 12$ h, while an equivalent exponential fed-batch process reaches its optimum $p_{pDNA} = 0.096\,g\,L\,h$ at $t^* = 3.3$ h. However, a linear fed-batch even without starvation outperforms an equivalent exponential fed-batch with (optimal) sulfate starvation as long as $\kappa_{pDNA} \leq 3.5$.

Typically, growth-decoupled processes suffer from a substantially decreasing (glucose) uptake rate during the production phase [42, 43]. Thus, our assumption of keeping an elevated q^*_{pDNA} constant over several hours may be unrealistic. Therefore, we investigated how the productivity optima change when the maximal feasible starvation length (t^*_{max}) is bounded. Yet, even in such cases, sulfate-limited fed-batches perform better than standard processes without starvation (Supplementary Figure S2).

3.4. Sulfate Limitation Experiments

The preceding analysis suggested that a three-stage process with sulfate starvation will deliver superior pDNA production performances compared to a two-stage, non-starved fed-batch process. To validate this prediction we set up a linear fed-batch process with *E. coli* JM108 as host (see Section 2.2 for details). Based on small molecule production rates during sulfate starvation [43, 44], we assumed a $\kappa_{pDNA} = 2$ and consequently predicted $t^* = 13$ h. Thus, we computed the initial SO_4^{2-} concentration to be $3.8\,g\,L^{-1}$ such that sulfate starvation occurs after 23 h in a 36 h bio-process.

Figure 5 highlights the feasibility of sulfur starvation to boost pDNA production in a (linear) fed-batch. Panel A illustrates the growth arrest due to sulfate starvation

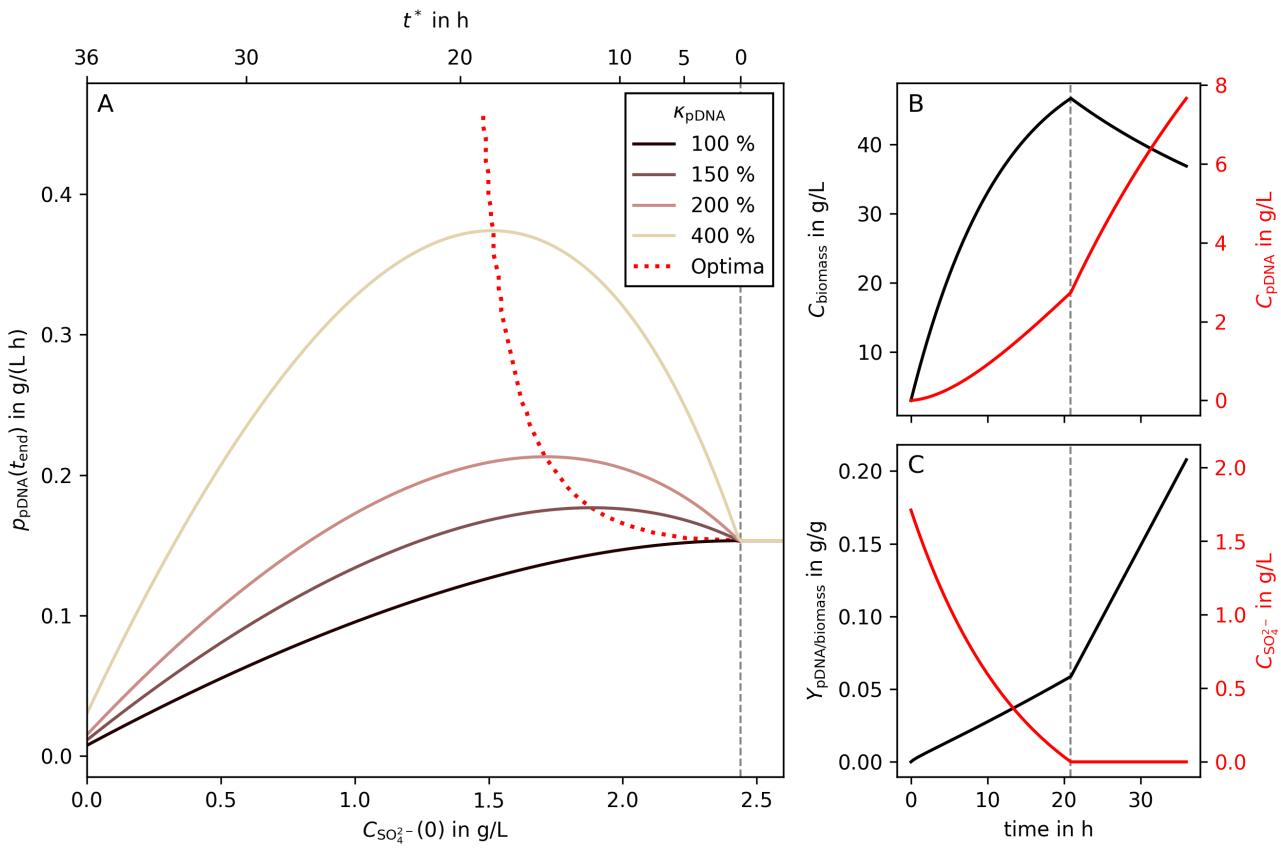

Figure 4: Predicted optimal timing in a SO_4^{2-}-limited linear fed-batch process. Panel **A** shows average volumetric productivities of pDNA production ($g\,L^{-1}\,h^{-1}$) as a function of the initial SO_4^{2-} concentration in a linear fed-batch process. The full line represents different levels of increased pDNA production during starvation as percentages of pDNA production rate during biomass growth (κ_{pDNA}). The dotted line indicates the location of the optima for κ_{pDNA} between 100 and 500 %. The second X-axis of panel **A** (top) illustrates the length of the sulfate-starved process phase (t^*). For all modeled linear fed-batch processes, right of the gray dashed line, no SO_4^{2-} limitation occurred. Panels **B** and **C** show the process curves of metabolites of interest in the optimal process for $\kappa_{pDNA} = 200\,\%$. The gray dashed lines indicate the switching time point between the growth and production phases.

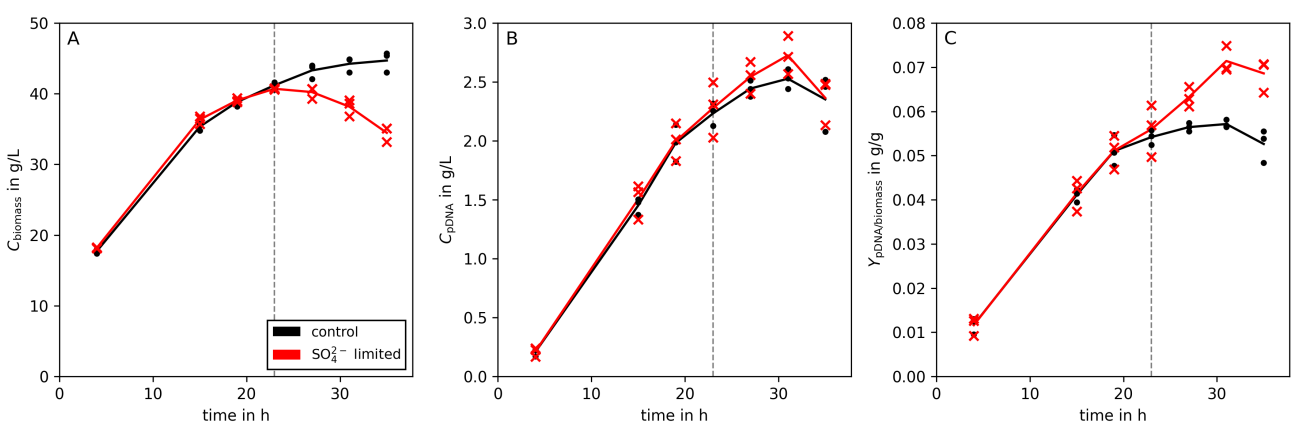

Figure 5: Experimental results of sulfate limitation. Panel **A** illustrates the biomass concentration, panel **B** the concentration of produced pDNA, and panel **C** the pDNA to biomass yield. Triplicates of the controls (no SO_4^{2-} limitation, black) and sulfate limited processes (red) are shown. Points correspond to individual observations; lines are calculated from the mean of the triplicates. The gray, dashed line represents the estimated time of the switch from biomass growth to pDNA production (projected at 23 h).

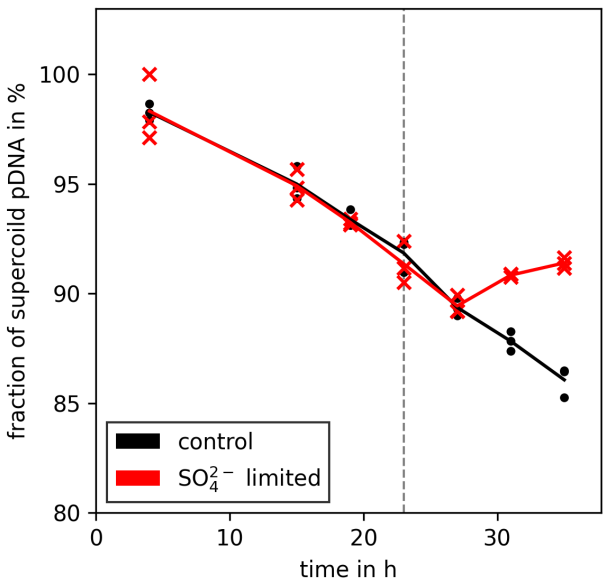

Figure 6: Fraction of supercoiled (ccc) pDNA over time for SO_4^{2-}-limited and control process. Experimental triplicates are shown as markers, full lines represent their mean.

(compare the diverging lines to the right of the dashed line). Due to dilution, the biomass concentration (red) decreases if cells no longer grow. Yet, pDNA concentration keeps rising–even faster than in the unstarved control (compare red with black control in panel B). Consequently, the specific pDNA yield rises too (panel C) reaching a maximum of 0.071 g g^{-1} after 31 h, which corresponds to an improvement of 25 % compared to control. The specific yield of supercoiled pDNA even increased by 29 %. However, beyond 31 h pDNA concentration and specific yield decrease in both the SO_4^{2-}-limited process as well as the control fermentation.

Moreover, we compared the fraction of pDNA present in a supercoiled conformation in the SO_4^{2-}-limited and control process (Figure 6). Until 27 h after induction, no differences are visible, thereafter, however, the SO_4^{2-}-limited process retains a higher fraction of supercoiled pDNA.

Next to the specific yield, also the average volumetric productivity increases by 8 % at 31 h (Figure 7A).

To investigate the unexpected behavior, we computed the specific productivities in the sulfate-limited and control fermentations (Figure 7B). In both bio-processes q_{pDNA} decreases with time which is in contrast to our modeling assumptions.

Finally, we compared the specific and volumetric yield achieved by the experiments in this study (at $t = 31$ h) to published values. Table 3 shows that the pDNA production strategy for our control values is already one of the best we could find, and with SO_4^{2-} limitation it performs better than all other published methods.

4. Discussion

Here we aimed to improve pDNA productivity by designing a three-stage bioprocess, where cellular growth and production are separated in time. Growth-decoupled processes are common design choices to enhance volumetric productivity in biochemical and biopharmaceutical production processes[43–46]. Especially with the advent of dynamic control in metabolic engineering that allows switching back and forth between metabolic growth and production phenotypes, interest in such (multi-stage) process designs has strongly grown [47]. Algorithms (e.g. MoVE [48]) that identify optimal metabolic switches are available. However, here we focused on easily implementable medium modifications that trigger the switching between growth and production.

In this study, we identified twelve possible decoupling components (SO_4^{2-}, K^+, Ca^{2+}, Cl^-, and compounds of trace elements) for the production of pDNA (Figure 1 and 2). All of them enable and regulate key functions in life [49]. Although trace elements act primarily as catalysts in enzyme systems, some of them, like copper and iron, play vital roles in energy metabolism [50]. However, we specifically selected SO_4^{2-} for further investigations because: (i) Sulfate is one of the six most prevalent elements in living organisms [41], which makes it comparably easy to measure and consequently determine the onset of starvation; (ii) Sulfate, in contrast to the other decoupling compounds, has a dedicated metabolic function that is well captured in the used genome-scale metabolic reconstruction *i*ML1515 of *E. coli*. [28]; (iii) Sulfate itself neither has a catalytic function nor a role in energy metabolism [51].

We simulated a three-stage fed-batch process where the transition from growth to production is triggered by the onset of sulfate starvation. Our computational model is based on two key assumptions: (i) In each phase the specific pDNA production rate is constant; (ii) pDNA productivity increases upon starvation, i.e. $\kappa_{\mathrm{pDNA}} = q^*_{\mathrm{pDNA}}/q^{\mu}_{\mathrm{pDNA}} > 1$. This aligns with experimental results of Masuda et al. [43], who reported a value of $\kappa_{\mathrm{melanovate}} = 1.16$ for melanovate production during sulfate-starvation. We find that sulfate starvation always results in improved pDNA production as long as $\kappa_{\mathrm{pDNA}} > 1$ independent of the specific bio-process (batch, exponential, or linear fed-batch). The length of starvation required to maximize volumetric productivity strongly depends on κ_{pDNA}.

Maintaining high pDNA productivity during sulfate starvation is a key requirement of our design. Our predictions are based on continuously elevated levels of pDNA productivity throughout the starvation phase. For long starvation phases, this may not be feasible [52]. However, Figure 8 illustrates that this assumption is not particularly crucial. In the worst case (at $\kappa_{\mathrm{pDNA}} = 160\,\%$), pDNA production needs to be maintained for 8.3 h to perform at least as well

Table 3: Comparison of pDNA specific yields and volumetric yields in published studies. The last two rows show the results of the experiments of this study (all pDNA conformations). Values marked with † are estimated from published figures. Values marked with ‡ are calculated from reported values. Values marked with ⋆ are converted from OD_{600} to cell dry mass (0.33 g/L/OD_{600}, BNID109838 [53]). Values reported as NA were not accessible.

Reference	yield		avg. vol.	biomass	pDNA	origin of	selection	*E. coli*	process
	specific [mg g^{-1}]	volumetric [mg L^{-1}]	productivity [mg L^{-1} h^{-1}]	conc. [g L^{-1}]	length [kbp]	replication	pressure	strain	type
[54]	10.8‡	58.3	3.9	5.4	NA	NA	ampicillin	BL21	shake flask
[11]	15 †⋆	57 †	8.2†‡	3.8‡	5.4	pUC	ampicillin	DH5α	shake flask
[13]	2.4†	8.0	0.8‡	3.3‡	3.0	pUC	kanamycin	BL21 *recA*-	batch
[55]	2.4	19.9	0.3	8.3‡	6.1	pUC	ampicillin	VH34	batch
[56]	2.4	30.0	2.7†‡	12.5‡	6.1	pUC	ampicillin	VH33	batch
[19]	7.0	230	17.7	34	3.9	pUC	kanamycin	DH5α	batch
[20]	7.9	35.9	2.3‡	4.6†	1.6	pUC	ampicillin	DH5α	batch
[57]	11.3	39.4	1.1†‡	3.5†	6.9	pUC	ampicillin	DH5α	batch
[17]	17.1‡	60	0.7‡	3.5	6.4	ColE1	none	JM109	batch
[16]	19.1	141	NA	7.4‡	3.7	pUC	kanamycin	GALG20	batch
[18]	32.4	102.8	NA	3.2	6.6	pBR322	ampicillin	VH33	batch
[10]	6.9‡	NA	NA	NA	6.9	pUC	ampicillin	W3110	continuous
[58]	1.6	33	3.0	20.6‡	4.0	pUC	none	DH5α	exp. fed-perfusion
[59]	10.1	74.8	3.1‡	8.3	2.4	pUC	kanamycin	PFC	fed-batch in shake flask
[12]	1.2	50	4.1	41	6.1	pUC	ampicillin	VH33	exp. fed-batch
[60]	7.6	25.6	NA	3.4‡	6.9	pUC	ampicillin	DH5α	exp. fed-batch
[57]	9.1	44	1.3‡	4.8‡	6.9	pUC	ampicillin	DH5α	exp./lin. fed-batch
[61]	9.5⋆	250	11.3†‡	26.4⋆	4.7	f1	kanamycin	DH5α	lin. fed-batch
[62]	9.8	140	3.9†‡	14.3‡	3.7	ColE1	kanamycin	GALG20	exp. fed-batch
[63]	31.2⋆	1923	72.4‡	62 ‡⋆	NA	pUC	ampicillin	BL21 *recA*$^-$	lin. fed-batch
[64]	15.5	759	31.2	49 ‡	3.9	pUC	kanamycin	DH5α	exp. fed-batch
[8]	25.9	939	35.1	36 ‡	3.5	ColE1	none	JM108*murselect*	exp. fed-batch
[62]	55.8†‡⋆	2177	41 †‡	39 †⋆	6.2	ColE1	kanamycin	GALG20	exp. fed-batch
[23]	51	2200	NA	43 ‡	6.5	pUC	kanamycin	DH5α	exp. fed-batch
[65]	65 ⋆	1830	42 †‡	28 ‡⋆	4.2	pUC	none	NTC4862	exp. fed-batch
[24]	68 ⋆	2590	NA	38 ‡⋆	6.2	pUC	kanamycin	DH5α	exp. fed-batch
control	57.1±0.7	2528 ±68	81.5±2.2	44.2±0.9	12.0	pUC	none	JM108	lin. fed-batch
SO_4^{2-} limited	71.4±2.5	2725 ±132	87.9±4.2	38.2±1.0	12.0	pUC	none	JM108	lin. fed-batch

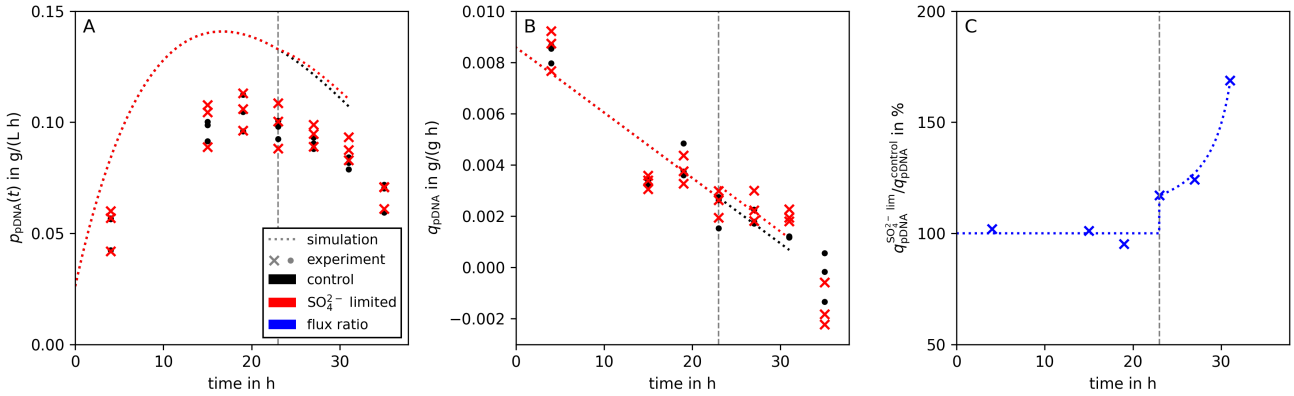

Figure 7: Calculated experimental rates and comparison to the simulation. Panel **A** illustrates the average volumetric productivity and panel **B** the pDNA production fluxes of control and SO_4^{2-}-limited process (black and red, respectively). Panel **C** shows the ratio of $q_{pDNA}^{SO_4^{2-}\ limited}$ and $q_{pDNA}^{control}$ (blue). Experimental triplicates are shown as markers, dotted lines are calculated from simulations. To adjust the simulations to the rates obtained in the experiments, a linearly decreasing $q_{pDNA}^{control}$ was fitted to experimental control data (black dotted line, panel **B**). Moreover, we fitted a parallel $q_{pDNA}^{SO_4^{2-}\ limited}$ (red dotted line, panel **B**) to conform to the experimental flux ratio (panel **C**). The vertical gray dashed line represents the estimated time of switching from biomass growth to pDNA production (projected at 23 h).

as a non-starved process. Our experimental data (Figure 5 and 7) demonstrate that this is indeed feasible. Interestingly, if κ_{pDNA} is raised beyond 160 %, the optimal starvation time increases too, but the minimally required length of pDNA production during starvation drops. This hints at a possible trade-off that may be explored in further process optimization steps.

During our validation experiments, we observed a decrease in the specific production of pDNA (Figure 7B), indicating that our initial modeling assumption of constant specific pDNA production rate throughout the feed and starvation phase was overly simplistic. Nevertheless, we consistently observed increased specific pDNA production rates during the starvation phase compared to the corresponding time points in the control (Figure 7C). This clear trend supports and validates our key assumption of $\kappa_{pDNA} > 1$ during starvation.

In an additional simulation performed after the validation experiments, we implemented a time-dependent q_{pDNA} and were able to show that the assumption of constant q_{pDNA} is not necessary for process improvements by SO_4^{2-} limitation (dotted lines in Figure 7 and Supplementary Figure S6). However, investigating why q_{pDNA} decreases throughout the process in more detail will be the scope of further work.

In a growth-decoupled process, it is essential to, first, reach high biomass which can subsequently catalyze product formation. With our process settings (i.e., fixed final process volume), this is best achieved with a linear feeding regime (Supplementary Figure S3), which quickly builds up biomass during the first few hours (compare Supplementary Figure S3B and E). In fact, we experimentally verified that a linear feeding strategy outperforms the exponential feed (data not shown). Interestingly a literature survey (Table 3) reveals that exponential feeding strategies are more frequently used.

A key challenge in any growth-decoupled process is to maintain metabolic activity in non-growing metabolic states. Often a strong decrease in nutrient uptake is observed [43]. However, during sulfate starvation, glucose concentration in the reactor remained below the detection limit, indicating that cells consistently maintained glucose uptake equal to the glucose feed rate. This supports the validity of our assumption stated in Equation 6. We speculate that this may be related to the fact that (i) due to the linear feed, the specific glucose uptake already dropped to 4 % of its initial value at the onset of starvation – 81 % lower than the (already) reduced specific uptake rate reported by Masuda et al. [43]; (ii) sulfate starvation retains high ATP-levels compared to other nutrient limitations [45, 66].

Consistent with maintained metabolic activity, we detect acetate accumulation during starvation (Supplementary Figure S5), which is a common sign of overflow metabolism in *E. coli* [67]. However, the theoretically predicted maximum acetate concentration overestimates the actually measured values, indicating the presence of alternative byproducts. Identifying these byproducts will be the focus of future investigations.

In both control and SO_4^{2-} limited experiments, specific pDNA yields and concentrations dropped at the end of the bioprocess. This might be due to other limitations (e.g., the O_2 transfer rate [68]), therefore, we suggest stopping the process at 31 h. Compared to the control, product concentration, average volumetric productivity, and specific yield at that point are up by 8 %, 8 %, and 25 %, respectively. Considering

the fraction of supercoiled pDNA, the sulfate-limited process gains another 4 %-points to all three performance indicators. Despite using a defined, minimal medium and a comparatively large plasmid (12 kbp) our process exceeds previously reported values [24] by 5 % in specific yield and volumetric yield (Table 3).

5. Conclusion

Based on genome-scale metabolic modeling we designed and successfully validated a three-stage (linear) fed-batch process for the production of pDNA in *E. coli* growing in a minimal medium. Switching between the growth and production phase was achieved by sulfate starvation. Upon sulfate starvation, the average volumetric productivity, specific pDNA yield, and supercoiled specific pDNA yield went up by 12 %, 25 %, and 29 %, respectively. Overall, our process achieved a specific pDNA yield of $71\,\mathrm{mg\,g^{-1}}$ and a volumetric yield of $2.7\,\mathrm{g\,L^{-1}}$ – an increase of more than 5 % compared to previous reports.

Declaration of Interest

MG and JZ received funding from enGenes Biotech GmbH and Baxalta Innovation GmbH, a part of Takeda companies. FS and FW are employees of enGenes Biotech GmbH. JM is one of the co-founders and Chief Executive Officer of enGenes Biotech GmbH. PG and BK are employees of Baxalta Innovation GmbH. Employees of Baxalta Innovations GmbH may be owners of stock and/or stock options. MG, JZ, FS, FW, and JM are authors of a patent application that has been filed on basis of the reported results.

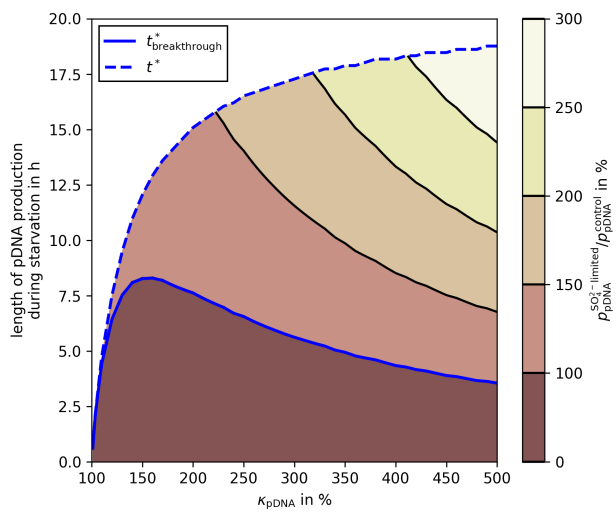

Figure 8: Breakthrough production length during starvation in linear fed-batch processes. If the pDNA production during starvation can be held longer than the breakthrough production length ($t^*_{\mathrm{breakthrough}}$, blue full line), the SO_4^{2-} limited process outperforms a control (i.e., not starved) process. A visual explanation of $t^*_{\mathrm{breakthrough}}$ is given in Supplementary Figure S4. The start of the starvation is defined by the optimal $C_{SO_4^{2-}}(0)$ calculated in Figure 4A (red dotted line). The maximum pDNA production length during starvation is equal to the total starvation length t^* (blue dashed line). The contour colors indicate the productivity of a SO_4^{2-} starved process compared to the control in % (color bar on the right).

CRediT authorship contribution statement

Mathias Gotsmy: Conceptualization, Methodology, Software, Formal Analysis, Investigation, Visualization, Writing – original draft, review and editing. **Florian Strobl:** Methodology, Formal Analysis, Investigation, Writing – review and editing. **Florian Weiß:** Methodology, Formal Analysis, Investigation, Writing – review and editing. **Petra Gruber:** Funding, Writing – review and editing. **Barbara Kraus:** Funding, Writing – review and editing. **Juergen Mairhofer:** Funding, Writing – review and editing. **Jürgen Zanghellini:** Conceptualization, Funding, Writing – original draft, review and editing.

References

[1] J. Mairhofer, A. R. Lara, Advances in host and vector development for the production of plasmid dna vaccines, in: Cancer Vaccines, Springer, 2014, pp. 505–541.

[2] European Medicines Agency, Comirnaty assessment report, https://www.ema.europa.eu/en/documents/assessment-report/comirnaty-epar-public-assessment-report_en.pdf, 2020. [Online; accessed 28-July-2022].

[3] A. Schmidt, H. Helgers, F. L. Vetter, A. Juckers, J. Strube, Fast and flexible mrna vaccine manufacturing as a solution to pandemic situations by adopting chemical engineering good practice—continuous autonomous operation in stainless steel equipment concepts, Processes 9 (2021) 1874.

[4] M. Ramamoorth, A. Narvekar, Non viral vectors in gene therapy-an overview, Journal of clinical and diagnostic research: JCDR 9 (2015) GE01.

[5] J.-Y. Cherng, N. Schuurmans-Nieuwenbroek, W. Jiskoot, H. Talsma, N. Zuidam, W. Hennink, D. Crommelin, Effect of dna topology on the transfection efficiency of poly ((2-dimethylamino) ethyl methacrylate)–plasmid complexes, Journal of controlled release 60 (1999) 343–353.

[6] L. Cupillard, V. Juillard, S. Latour, G. Colombet, N. Cachet, S. Richard, S. Blanchard, L. Fischer, Impact of plasmid supercoiling on the efficacy of a rabies dna vaccine to protect cats, Vaccine 23 (2005) 1910–1916.

[7] D. S. Cunningham, R. R. Koepsel, M. M. Ataai, M. M. Domach, Factors affecting plasmid production in escherichia coli from a resource allocation standpoint, Microbial cell factories 8 (2009) 1–17.

[8] J. Mairhofer, M. Cserjan-Puschmann, G. Striedner, K. Nöbauer, E. Razzazi-Fazeli, R. Grabherr, Marker-free plasmids for gene therapeutic applications—lack of antibiotic resistance gene substantially improves the manufacturing process, Journal of biotechnology 146 (2010) 130–137.

[9] D. M. Bower, K. L. Prather, Engineering of bacterial strains and vectors for the production of plasmid dna, Applied microbiology and biotechnology 82 (2009) 805–813.

[10] M. Wunderlich, H. Taymaz-Nikerel, G. Gosset, O. T. Ramírez, A. R. Lara, Effect of growth rate on plasmid dna production and metabolic performance of engineered escherichia coli strains, Journal of bioscience and bioengineering 117 (2014) 336–342.

[11] J. Galindo, B. L. Barrón, A. R. Lara, Improved production of large plasmid dna by enzyme-controlled glucose release, Annals of Microbiology 66 (2016) 1337–1342.

[12] R. Soto, L. Caspeta, B. Barrón, G. Gosset, O. T. Ramírez, A. R. Lara, High cell-density cultivation in batch mode for plasmid dna production by a metabolically engineered e. coli strain with minimized overflow metabolism, Biochemical engineering journal 56 (2011) 165–171.

[13] K. E. Jaén, D. Velazquez, F. Delvigne, J.-C. Sigala, A. R. Lara, Engineering e. coli for improved microaerobic pdna production, Bioprocess and biosystems engineering 42 (2019) 1457–1466.

[14] A. R. Lara, K. E. Jaén, O. Folarin, E. Keshavarz-Moore, J. Büchs, Effect of the oxygen transfer rate on oxygen-limited production of plasmid dna by escherichia coli, Biochemical Engineering Journal 150 (2019) 107303.

[15] D. S. Cunningham, Z. Liu, N. Domagalski, R. R. Koepsel, M. M. Ataai, M. M. Domach, Pyruvate kinase-deficient escherichia coli exhibits increased plasmid copy number and cyclic amp levels, Journal of bacteriology 191 (2009) 3041–3049.

[16] G. A. Gonçalves, D. M. Prazeres, G. A. Monteiro, K. L. Prather, De novo creation of mg1655-derived e. coli strains specifically designed for plasmid dna production, Applied microbiology and biotechnology 97 (2013) 611–620.

[17] Z. Wang, G. Le, Y. Shi, G. Wegrzyn, Medium design for plasmid dna production based on stoichiometric model, Process Biochemistry 36 (2001) 1085–1093.

[18] L. Martins, A. Pedro, D. Oppolzer, F. Sousa, J. Queiroz, L. Passarinha, Enhanced biosynthesis of plasmid dna from escherichia coli vh33 using box–behnken design associated to aromatic amino acids pathway, Biochemical Engineering Journal 98 (2015) 117–126.

[19] F. Islas-Lugo, J. Vega-Estrada, C. A. Alvis, J. Ortega-Lopez, M. del Carmen Montes-Horcasitas, Developing strategies to increase plasmid dna production in escherichia coli dh5α using batch culture, Journal of biotechnology 233 (2016) 66–73.

[20] M. K. Danquah, G. M. Forde, Growth medium selection and its economic impact on plasmid dna production, Journal of bioscience and bioengineering 104 (2007) 490–497.

[21] A. Kay, R. O'Kennedy, J. Ward, E. Keshavarz-Moore, Impact of plasmid size on cellular oxygen demand in escherichia coli, Biotechnology and applied biochemistry 38 (2003) 1–7.

[22] O. Folarin, D. Nesbeth, J. M. Ward, E. Keshavarz-Moore, Application of plasmid engineering to enhance yield and quality of plasmid for vaccine and gene therapy, Bioengineering 6 (2019) 54.

[23] J. A. Williams, J. Luke, S. Langtry, S. Anderson, C. P. Hodgson, A. E. Carnes, Generic plasmid dna production platform incorporating low metabolic burden seed-stock and fed-batch fermentation processes, Biotechnology and bioengineering 103 (2009) 1129–1143.

[24] A. E. Carnes, J. M. Luke, J. M. Vincent, A. Schukar, S. Anderson, C. P. Hodgson, J. A. Williams, Plasmid dna fermentation strain and process-specific effects on vector yield, quality, and transgene expression, Biotechnology and bioengineering 108 (2011) 354–363.

[25] K. E. Jaén, A. R. Lara, O. T. Ramírez, Effect of heating rate on pdna production by e. coli, Biochemical engineering journal 79 (2013) 230–238.

[26] G. Monteiro, S. Duarte, M. Martins, S. Andrade, D. Prazeres, High copy number plasmid engineering for biopharmaceutical-grade pdna production in lactococcus lactis, Journal of Biotechnology 305 (2019) S23–S24.

[27] S. O. Duarte, G. A. Monteiro, Plasmid replicons for the production of pharmaceutical-grade pdna, proteins and antigens by lactococcus lactis cell factories, International Journal of Molecular Sciences 22 (2021) 1379.

[28] J. M. Monk, C. J. Lloyd, E. Brunk, N. Mih, A. Sastry, Z. King, R. Takeuchi, W. Nomura, Z. Zhang, H. Mori, et al., i ml1515, a knowledgebase that computes escherichia coli traits, Nature biotechnology 35 (2017) 904–908.

[29] A. Ebrahim, J. A. Lerman, B. O. Palsson, D. R. Hyduke, Cobrapy: constraints-based reconstruction and analysis for python, BMC systems biology 7 (2013) 1–6.

[30] F. C. Neidhardt, J. L. Ingraham, M. Schaechter, Physiology of the bacterial cell; a molecular approach, 589.901 N397, Sinauer associates, 1990.

[31] N. E. Lewis, K. K. Hixson, T. M. Conrad, J. A. Lerman, P. Charusanti, A. D. Polpitiya, J. N. Adkins, G. Schramm, S. O. Purvine, D. Lopez-Ferrer, et al., Omic data from evolved e. coli are consistent with computed optimal growth from genome-scale models, Molecular systems biology 6 (2010) 390.

[32] R. Mahadevan, J. S. Edwards, F. J. Doyle III, Dynamic flux balance analysis of diauxic growth in escherichia coli, Biophysical journal 83 (2002) 1331–1340.

[33] K. Höffner, S. M. Harwood, P. I. Barton, A reliable simulator for dynamic flux balance analysis, Biotechnology and bioengineering 110 (2013) 792–802.

[34] P. Virtanen, R. Gommers, T. E. Oliphant, M. Haberland, T. Reddy, D. Cournapeau, E. Burovski, P. Peterson, W. Weckesser, J. Bright, et al., Scipy 1.0: fundamental algorithms for scientific computing in python, Nature methods 17 (2020) 261–272.

[35] P. Wong, S. Gladney, J. D. Keasling, Mathematical model of the lac operon: inducer exclusion, catabolite repression, and diauxic growth on glucose and lactose, Biotechnology progress 13 (1997) 132–143.

[36] A. Varma, B. O. Palsson, Stoichiometric flux balance models quantitatively predict growth and metabolic by-product secretion in wild-type escherichia coli w3110, Applied and environmental microbiology 60 (1994) 3724–3731.

[37] C. Yanisch-Perron, J. Vieira, J. Messing, Improved m13 phage cloning vectors and host strains: nucleotide sequences of the m13mpl8 and puc19 vectors, Gene 33 (1985) 103–119.

[38] H. C. Bimboim, J. Doly, A rapid alkaline extraction procedure for screening recombinant plasmid dna, Nucleic acids research 7 (1979) 1513–1523.

[39] B. Dahlgren, O. Čertík, finitediff, 2021. URL: https://github.com/bjodah/finitediff. doi:https://dx.doi.org/10.5281/zenodo.5168369.

[40] B. Fornberg, Classroom note: Calculation of weights in finite difference formulas, SIAM review 40 (1998) 685–691.

[41] H. C. Lange, J. J. Heijnen, Statistical reconciliation of the elemental and molecular biomass composition of Saccharomyces cerevisiae, Biotechnology and Bioengineering 75 (2001) 334–344.

[42] S. Klamt, R. Mahadevan, O. Hädicke, When do two-stage processes outperform one-stage processes?, Biotechnology journal 13 (2018) 1700539.

[43] A. Masuda, Y. Toya, H. Shimizu, Metabolic impact of nutrient starvation in mevalonate-producing escherichia coli, Bioresource technology 245 (2017) 1634–1640.

[44] C. Willrodt, A. Hoschek, B. Bühler, A. Schmid, M. K. Julsing, Decoupling production from growth by magnesium sulfate limitation boosts de novo limonene production, Biotechnology and Bioengineering 113 (2016) 1305–1314.

[45] K. Tokuyama, Y. Toya, F. Matsuda, B. F. Cress, M. A. Koffas, H. Shimizu, Magnesium starvation improves production of malonyl-coa-derived metabolites in escherichia coli, Metabolic engineering 52 (2019) 215–223.

[46] P. Stargardt, L. Feuchtenhofer, M. Cserjan-Puschmann, G. Striedner, J. Mairhofer, Bacteriophage inspired growth-decoupled recombinant protein production in escherichia coli, ACS Synthetic Biology 9 (2020) 1336–1348.

[47] C. J. Hartline, A. C. Schmitz, Y. Han, F. Zhang, Dynamic control in metabolic engineering: Theories, tools, and applications, Metabolic Engineering 63 (2021) 126–140.

[48] N. Venayak, A. von Kamp, S. Klamt, R. Mahadevan, MoVE identifies metabolic valves to switch between phenotypic states, Nature Communications 9 (2018) 5332.

[49] W. Maret, P. Blower, Teaching the chemical elements in biochemistry: Elemental biology and metallomics, Biochemistry and Molecular Biology Education 50 (2022) 283–289.

[50] N. R. C. U. C. o. D. a. Health, Trace Elements, in: Diet and Health: Implications for Reducing Chronic Disease Risk, National Academies Press (US), 1989, p. 301. URL: https://www.ncbi.nlm.nih.gov/books/NBK218751/.

[51] D. Markovich, Physiological roles and regulation of mammalian sulfate transporters, Physiological reviews 81 (2001) 1499–1533.
[52] A. St John, A. Goldberg, Effects of starvation for potassium and other inorganic ions on protein degradation and ribonucleic acid synthesis in escherichia coli, Journal of bacteriology 143 (1980) 1223–1233.
[53] R. Milo, P. Jorgensen, U. Moran, G. Weber, M. Springer, Bionumbers—the database of key numbers in molecular and cell biology, Nucleic acids research 38 (2010) D750–D753.
[54] Z.-N. Xu, W.-h. Shen, H. Chen, P.-l. Cen, Effects of medium composition on the production of plasmid dna vector potentially for human gene therapy, Journal of Zhejiang University. Science. B 6 (2005) 396.
[55] T. E. Pablos, R. Soto, E. M. Mora, S. Le Borgne, O. T. Ramírez, G. Gosset, A. R. Lara, Enhanced production of plasmid dna by engineered escherichia coli strains, Journal of biotechnology 158 (2012) 211–214.
[56] J. T. Cortés, N. Flores, F. Bolívar, A. R. Lara, O. T. Ramírez, Physiological effects of ph gradients on escherichia coli during plasmid dna production, Biotechnology and bioengineering 113 (2016) 598–611.
[57] A. Dorward, R. D. O'Kennedy, O. Folarin, J. M. Ward, E. Keshavarz-Moore, The role of amino acids in the amplification and quality of dna vectors for industrial applications, Biotechnology Progress 35 (2019) e2883.
[58] A. García-Rendón, R. Munguía-Soto, R. M. Montesinos-Cisneros, R. Guzman, A. Tejeda-Mansir, Performance analysis of exponential-fed perfusion cultures for pdna vaccines production, Journal of Chemical Technology & Biotechnology 92 (2017) 342–349.
[59] M. de la Cruz, E. A. Ramírez, J.-C. Sigala, J. Utrilla, A. R. Lara, Plasmid dna production in proteome-reduced escherichia coli, Microorganisms 8 (2020) 1444.
[60] R. D. O'Kennedy, J. M. Ward, E. Keshavarz-Moore, Effects of fermentation strategy on the characteristics of plasmid dna production, Biotechnology and applied biochemistry 37 (2003) 83–90.
[61] K. O'Mahony, R. Freitag, F. Hilbrig, P. Müller, I. Schumacher, Strategies for high titre plasmid dna production in escherichia coli dh5α, Process Biochemistry 42 (2007) 1039–1049.
[62] G. A. Goncalves, K. L. Prather, G. A. Monteiro, A. E. Carnes, D. M. Prazeres, Plasmid dna production with escherichia coli galg20, a pgi-gene knockout strain: Fermentation strategies and impact on downstream processing, Journal of biotechnology 186 (2014) 119–127.
[63] J.-N. Phue, S. J. Lee, L. Trinh, J. Shiloach, Modified escherichia coli b (bl21), a superior producer of plasmid dna compared with escherichia coli k (dh5α), Biotechnology and bioengineering 101 (2008) 831–836.
[64] F. Grijalva-Hernández, J. Vega-Estrada, M. Escobar-Rosales, J. Ortega-López, R. Aguilar-López, A. R. Lara, M. d. C. Montes-Horcasitas, High kanamycin concentration as another stress factor additional to temperature to increase pdna production in e. coli dh5α batch and fed-batch cultures, Microorganisms 7 (2019) 711.
[65] J. Nelson, S. Rodriguez, N. Finlayson, J. Williams, A. Carnes, Antibiotic-free production of a herpes simplex virus 2 dna vaccine in a high yield cgmp process, Human Vaccines & Immunotherapeutics 9 (2013) 2211–2215.
[66] V. Chubukov, U. Sauer, Environmental dependence of stationary-phase metabolism in bacillus subtilis and escherichia coli, Applied and environmental microbiology 80 (2014) 2901–2909.
[67] E. El-Mansi, W. Holms, Control of carbon flux to acetate excretion during growth of escherichia coli in batch and continuous cultures, Microbiology 135 (1989) 2875–2883.
[68] A. Castan, S.-O. Enfors, Characteristics of a do-controlled fed-batch culture of escherichia coli, Bioprocess Engineering 22 (2000) 509–515.